REPORT FOR OPEN LAB PROJECT

INFLUENCE OF SURFACE CONDITIONS AND ANGLES OF ATTACK ON AIRBRAKE DRAG

Prepared by: Division 1, Team 19
Agathiya Tharun (atharun@purdue.edu)
Joe Misenar (jmisenar@purdue.edu)
Pranav Madhavan (pmadhava@purdue.edu)

School of Mechanical Engineering,
Purdue University
585 Purdue Mall
West Lafayette, IN 47907

Date: 2023.04.18

Submitted to: Prof. Jun Chen

1 INTRODUCTION

Liftoff is the most challenging aspect of a rocket launch for aerospace engineers to consider. The airbrakes on a rocket play a crucial role in the success of its launch and deployment. Not only are they important to help control the drag acting on the rocket, but according to the Kerbal Space Program, it is also extremely important in helping steer the rocket in a particular direction as well as controlling its speed ("A.I.R.B.R.A.K.E.S", 2023). This experiment aims to characterize the drag force acting on a rocket during its ascent. This is particularly applicable to the Purdue Space Program, as its Spaceport America team is in the process of designing SED's first-ever airbrake system. PSP is currently facing the concern of an overshot apogee and hopes to use an airbrake to slow its ascent and prevent an overshot apogee.

An important aspect of drag is boundary layer separation. Boundary layers are regions near a boundary where there are significant viscous effects. The boundary layer separation point is the point at which the boundary layer no longer contours the surface of the body and leads to the formation of a wake region ("Flow Separation", 2020). Turbulent flow, where the Reynolds number is greater than 500,000, delays boundary layer separation, resulting in a smaller wake with a more symmetric pressure profile, which in turn reduces the form drag acting on the body.

The non-dimensional Reynolds number characterizes the ratio of inertial to viscous forces and can be found using the following equation.

$$R_e = \frac{\rho V_o D}{\mu} \quad \text{Eqn. 1.1}$$

where R_e is Reynolds number, ρ is density, V_o is freestream velocity, D is the characteristic model size, and μ is the dynamic viscosity of air.

The ideal gas law was used to determine the air density, ρ, using atmospheric pressure, P_{atm}, the ideal gas constant for air, R_{air}, and the temperature, T:

$$\rho = \frac{P_{atm}}{R_{air} T} \quad \text{Eqn. 1.2}$$

The ideal gas constant for air can be determined by dividing the ideal gas constant by the molar mass of air.

The expression for drag force can be found as:

$$F_D = \frac{1}{2} \rho V_o^2 A C_D \quad \text{Eqn. 1.3}$$

where F_D is the drag force acting on the body, ρ is density, V_o is freestream velocity, A is area, and C_D is the coefficient of drag.

For this experiment, air density was assumed to be constant regardless of the altitude of the rocket. Furthermore, the air brake was assumed to be a streamlined body instead of a bluff one. The reasoning behind this is elaborated on in the discussion section.

1.1 Dimensional Analysis

Dimensional Analysis is an analytical tool used to reduce the number and complexity of variables used to describe a physical system and is very heavily used in the field of fluid mechanics. In fluid mechanics experiments, tests are often carried out on smaller-scale models of a given prototype and the results are then adjusted to the full-scale prototype. For example, in professional

racing, tests are often done on small-scale models of a car in smaller wind tunnels to measure drag and wind flow over the car. Adjustments to designs are then made based on the results of the experiments followed by more testing until finally, a full-scale prototype is built. Using dimensional analysis in this way allows companies to save money and resources until a more reliable design is made.

However, in order to perform dimensional analysis, three requirements must be met: geometric similarity, kinematic similarity, and dynamic similarity. Geometric similarity refers to the condition where the prototype and model have the same shape so that all linear dimensions can be related by a constant scaling factor. Kinematic similarity refers to the condition that flow velocities at any given point on the model and prototype have the same direction and can be related by a constant scaling factor. Finally, dynamic similarity refers to the condition that the ratio of forces in the model is the same as the ratio of significant forces in the prototype. For example, the model and prototype must have the same Reynolds number, Strouhal number, Froude number, etc.

The team has assumed geometric, kinematic, and dynamic similarity for this experiment. This is an extremely important assumption as without it, the results of testing on the model cannot be extrapolated to the prototype being used by PSP.

1.2 Force Measurement

The wind tunnel used in this experiment is equipped with a dynamometer on the bottom of the test section which is used to measure the drag forces on the test model. As the test is run, forces are generated by the test model which causes slight deflections in the beam assemblies in the test section. The deflections are detected by a linear variable differential transform (LVDT), which converts the motion of an object to an electrical signal. The LVDT outputs voltages which are then related to forces using the following relationship:

$$F = K * [(V_{total} - V_{0,offset,total}) - (V_{ts} - V_{0,offset,ts})] \quad \text{Eqn. 1.2.1}$$

The following variables are referenced in the equation above:

- F: modified drag force (Newtons).
- V_{total}: Total voltage at test condition (Volts).
- $V_{0,offset,total}$: Voltage reading at 0 wind speed with both the test model and stand (Volts).
- V_{ts}: Voltage reading with test stand only at the test condition (Volts).
- $V_{0,offset,ts}$: Voltage reading with test stand only at zero wind speed (Volts).
- K: Calibration constant.

1.3 Drag Coefficient

The drag coefficient is a dimensionless form of expressing drag, and can be found using the following relationship:

$$C_D = \frac{F_D}{\frac{1}{2}\rho V_o^2 A} \quad \text{Eqn. 1.3.1}$$

The following variables are referenced in the equation above:

- C_D: Drag coefficient (unitless)
- F_D: Drag force (newtons)

- ρ: Density of air at the given test conditions in $\frac{kg}{m^3}$
- V_O: Freestream velocity in $\frac{m}{s}$
- A: Frontal projected area in m^2

2 OBJECTIVE

The team's objective is to characterize the drag experienced on proposed airbrake designs by measuring the drag on various test configurations. The Purdue Space Program's Spaceport America team is in the process of designing SEDS' first-ever airbrake system. The results will then be used with dimensional analysis to extrapolate data for the true conditions the airbrake will experience at higher velocities. The goal for this lab is to find the conditions to maximize the drag acting on the air brake, such that PSP's Spaceport America team will not overshoot the intended apogee.

3 METHOD

3.1 Experiment Facility

The Open Lab was conducted in a low-speed open-circuit wind tunnel (ELD Model 402B, **Fig. 3.1**). The airbrake model was mounted in a test section that experiences uniform and clean incoming airflow. **Fig. 3.2** shows the test section with dimensions of 30.5 cm (width) × 30.5 cm (height) × 61 cm (length), and the model airbrake used in the open lab. The wind speed was set at 60Hz (44.66 m/s) using a variable frequency drive (VFD) that adjusts the rotation of the belt-driven fan at different speeds.

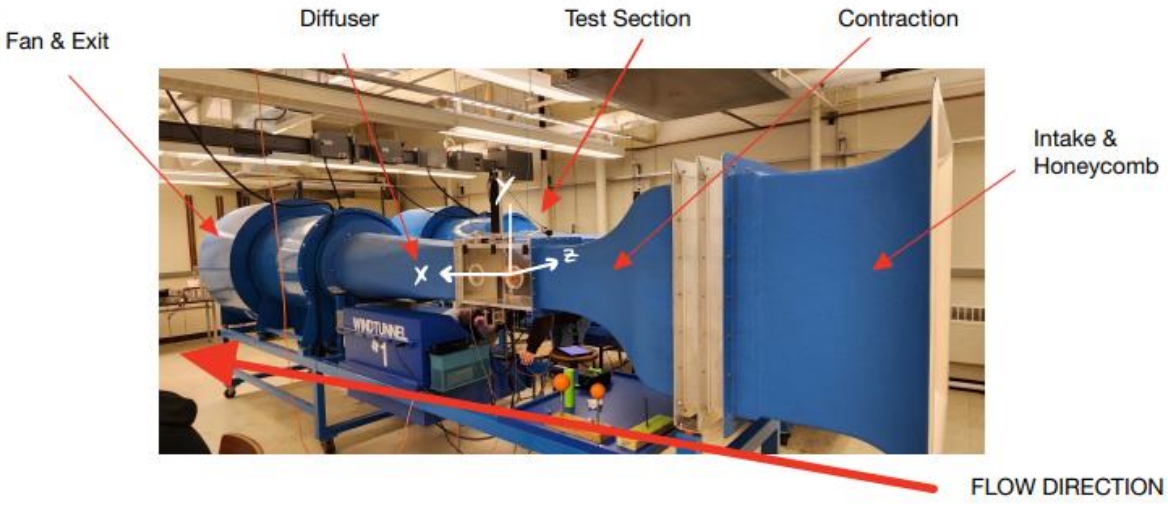

Fig. 3.1 Wind tunnel used for this lab at the Mechanical Engineering Building.

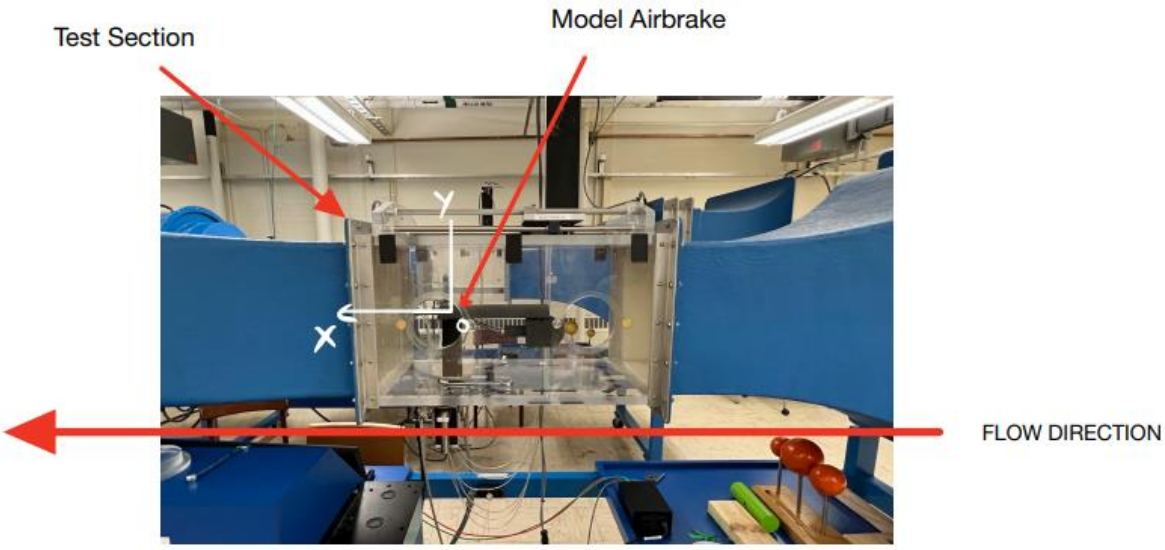

Fig. 3.2 Test section with model airbrake used in this lab.

3.2 Test Model

The team's model consists of an all-thread rod, a hub, a calibration jig, and an airbrake. The all-thread rod (**Fig 3.6)** was bent in such a way that it could be threaded into the LVDT mount and into the test model hub so that it was offset both upstream and along the negative y-axis to avoid interference with the ceiling of the test section while the airbrake is set to high angles of attack. The hub was made with internal teeth so that either the jig or airbrake could slide into it with their external teeth. Each tooth increment is equivalent to a 5° angle change. The purpose of the jig is to zero out the frontal projected area as well as for mounting purposes as seen in **Fig. 3.4**. It is not part of the airbrake itself. Hence, the jig has no airbrake attached to it. The airbrake with a rough surface is seen below in **Fig. 3.5**. This design has sandpaper attached to its surface to induce turbulent flow. The airbrake with a smooth surface is seen below in **Fig. 3.3**, which induces laminar flow. **Fig. 3.6** shows the entire airbrake test model in the positive 30° position.

Fig. 3.3 Standalone airbrake model.

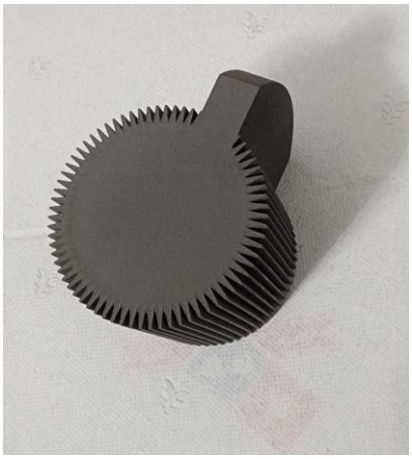

Fig. 3.4 Calibration jig.

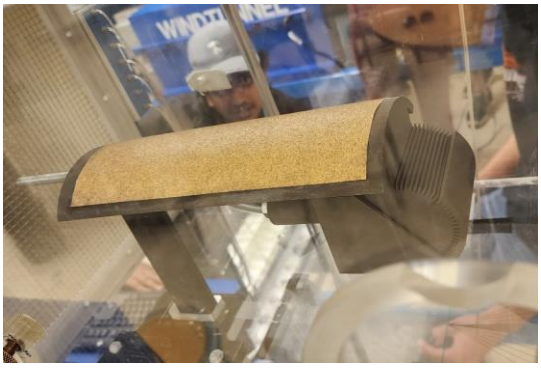

Fig. 3.5 Rough airbrake for turbulent flow.

3.3 Instrumentation

1. Dynamometer

A Dynamometer is mounted on the bottom floor of the test section and measures lift and drag forces applied to the test model along two axes. The forces generated by the model deflect the supportive strut on the assembly. This deflection is detected by a linear variable differential transform (LVDT), which converts deflection into a corresponding electrical signal, and can then be measured as a force. The range of the device is 0 to 100N for lift and drag.

2. Data Acquisition System

A data acquisition system (National Instrument USB-6210) is installed to collect data from all of the different instruments. The system is capable of reading up to 32 analog inputs at 16 bits and producing up to 2 analog outputs at 16 bits. The system offers analog I/O, digital I/O, and 16-bit counters and timers. The system reads the pressure difference signal from the differential pressure transducers, the pressure signal from the pressure sensors, and the flow rate signal from the flow meters. LabView Software is used to control the data acquisition system.

3. Bechtel Innovation Design Center

The Bechtel Innovation Design Center will also be utilized for the open lab. This includes using the Fuse 1 Nylon 3D printer to print certain parts. These machines will be readily available and will be adequate for the said lab.

4. Mallott Machine Shop

The Mechanical Engineering Building's Mallott Prototyping Lab contains vices, handheld tools, sandpaper, wrenches, and glue. Such resources can be utilized for making finer changes to the test model.

3.4 Experimental Conditions

In this lab, the wind tunnel produces flow at a velocity of 44.66 m/s when the Variable Frequency Drive is set to a frequency of 60Hz. However, in order to record the zero offset of the drag signal, the VFD is set at 0Hz to allow the wind tunnel to produce zero airflow. The calibration jig is then inserted into the hub to allow for calibration measurements. The hub model was installed at the center of the wind tunnel as shown in **Fig. 3.6**. The airbrake slides into the hub and was tested at seven different angles ranging from 0° to 30° in increments of 5°.

The drag forces are measured by the LVDT which is connected to the model support and is located underneath the test section. The Reynolds number in the present lab is 217,934.

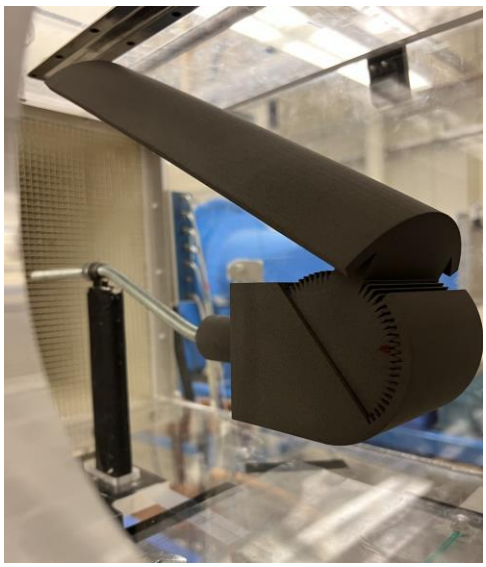

Fig. 3.6 Full Test Model and LVDT used in this lab.

The aforementioned experimental conditions and their corresponding values are summarized in the table below (**Tab. 3.1**):

Experimental Condition	**Value**
Wind speed	44.66 [m/s]
Angles of attack	[0°, 5°, 10°, 15°, 20°, 25°, 30°]
Dimension of airbrake	10×3.28 [inches]
Reynolds number	217,934

Table 3.1 Experimental Conditions Table.

3.5 Procedures

This section describes the procedure followed to conduct this experiment. Firstly, the zero offsets of the drag signal should be measured with the all-thread rod, hub, and calibration jig in the test section. A recording at 0Hz should be recorded. Next, measurements should be recorded at 60Hz (44.66 m/s) at angles of 0° to 30° in increments of 5° with only the calibration jig inserted into the hub. There should be an allowed 15 seconds between runs in order for the model and airflow to settle and reach a steady state. This helps prevent noise, vibration effects, and other errors. In order to offset the weight of the airbrake, measurements should be taken at 0Hz at angles of 0° to 30° in increments of 5° with only the airbrake inserted into the hub. This improves the accuracy of the drag data since the moment on the LVDT caused by the weight of the airbrake changes as the airbrake changes its angle of attack. It should be noted that these zero offsets can also be used to calibrate data from the turbulence-inducing airbrake model since the sandpaper attached to serve as a rough surface is considered to have negligible weight. Next, drag measurements should be taken with the smooth-surfaced airbrake inserted into the hub to induce laminar flow. These measurements are taken at 60Hz and at angles of 0° to positive 30° in increments of °. This should be repeated for the airbrake with a rough surface that induces turbulent flow. After all measurements are taken, the wind tunnel should be turned off. It should be noted that depending on the size of the test section, a bent all-thread rod may need to be utilized to lower the model within the space to prevent it from interfering with the test section at higher angles of attack due to its enlarged volume.

4 RESULTS

The raw data collected from the LVDT were voltage values. Data was collected under various conditions to ensure that the influence of the test stand on the model's drag results were negated. Using **Eqn. 1.2.1**, drag forces were computed for the two models that were tested. The first model had a smooth surface to induce a laminar air flow. The second model was layered with sandpaper to create a rougher surface to induce turbulent air flow. The drag force results for both models at various angles of attack can be seen below in **Fig. 4.1**:

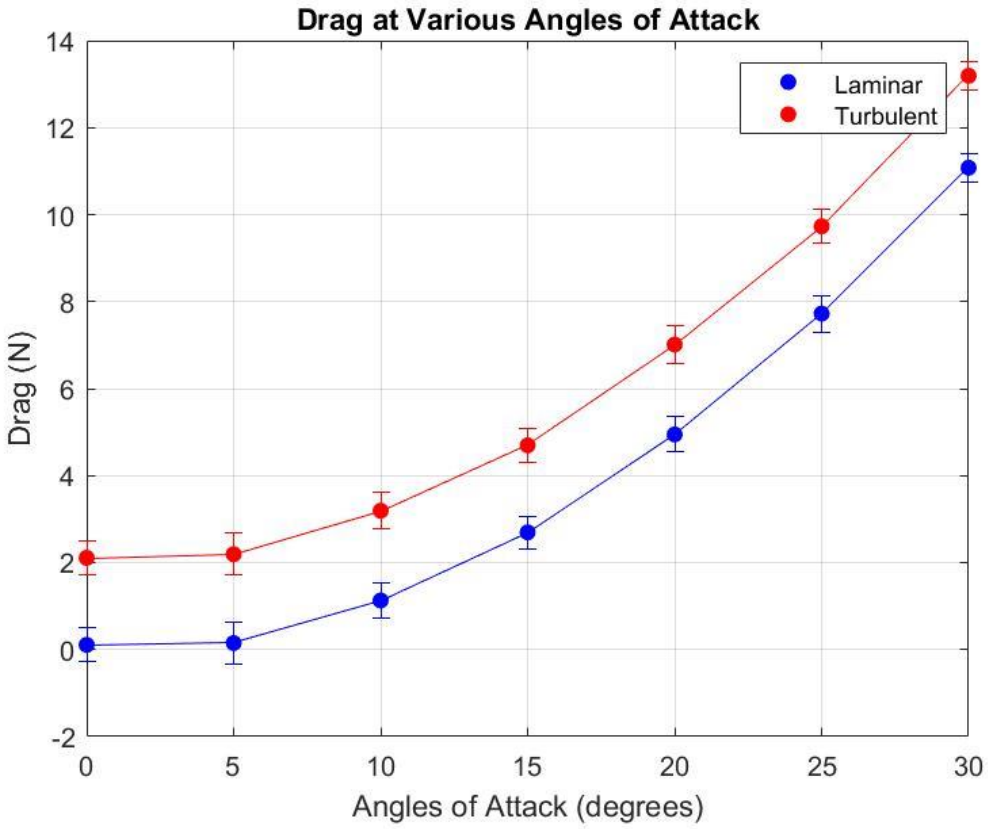

Fig. 4.1 Drag force as a function of angle of attack for laminar and turbulent flow.

In order to characterize the results in terms of the coefficient of drag, the data was recomputed through an algorithm the team created on MATLAB. The results of how the coefficient of drag value changed with angle of attack and surface conditions can be seen below in **Fig. 4.2**:

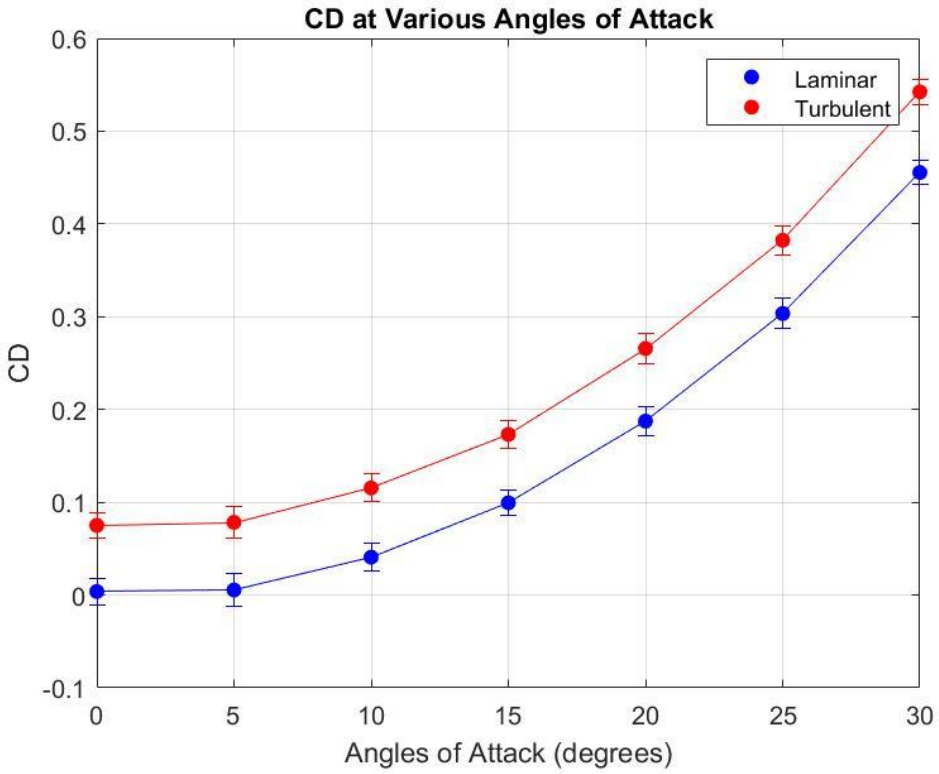

Fig. 4.2 Coefficient of drag as a function of angle of attack for laminar and turbulent flow.

In both **Fig. 4.1** and **Fig. 4.2**, it can clearly be seen that drag is maximized at larger angles of attack and under turbulent airflow. Since the experiment was conducted with a true-sized replica model of the airbrake intended to be used on the actual rocket, the data collected can easily be extrapolated, using dimensional analysis, to predict the amount of drag force the rocket can experience at higher velocities. This data clearly informs the PSP Spaceport America team that the ideal design for maximizing drag is to maintain a large angle of attack with a rough surface to induce turbulent flow. Therefore, the goals of this experiment have successfully been met.

The implications of this data are significant. By knowing exactly how much drag can be reduced, the team can properly dictate the duration for which the airbrake should be deployed such that enough drag is generated to reduce the rocket's apogee by the intended amount.

A variety of external factors, measurement uncertainty, unaccounted forces, and experimental setup errors led to errors in the experimental data, however. As seen above, each figure has uncertainty bars at each of the data points. These error bars represent the range of possible values that could theoretically represent the true data point. Due to device and measurement uncertainty, the measured voltage values are prone to errors in their readings. The magnitude of the device and measurement uncertainties are taken and passed through an error propagation formula that accounts for the error being compounded when solving for the drag coefficient. This uncertainty is represented through the error bars at each data point. This error includes voltage measurement, LVDT device uncertainty, and error propagation into the force and drag coefficient equations.

5 DISCUSSION

As seen in **Fig. 4.1** and **Fig. 4.2**, the drag force and coefficient of drag increase exponentially as the angle of attack increases. These results are consistent with the drag force expression found in **Eqn. 1.3** – as the frontal projected area increases with the angle of attack, so does drag force. It can also be seen that the drag is significantly higher for turbulent flow compared to laminar flow. This is because turbulent flow carries larger velocities close to the wall and thus has more momentum. Due to this higher momentum, turbulent flow can travel further through an adverse pressure gradient before the boundary layer separates. In addition to delaying boundary layer separation compared to laminar flow, turbulent flow creates a smaller wake. A lower wake area increases the pressure behind the body causing the pressure difference between the entrance and wake to be less, thus reducing form drag. For a bluff body, form drag is the largest contributor – reducing this form drag with a turbulent flow causes the total drag to decrease despite the increase in skin friction drag that results from the turbulent airflow. The team's assumption that the airbrake can be treated as a streamline body can thus be justified. As seen in **Fig. 4.1**, the airbrake experiences more drag under turbulent flow. This is inconsistent with the idea that bluff bodies experience less drag under turbulent flow. Therefore, the airbrake, even at an angle of attack of 30°, can be treated as a streamline body. Thus, the team's calculations for the coefficient of drag, which depended on this area, can be observed as being an accurate representation of the model.

The range of drag force for the laminar flow environment is [0.394, 11.078] Newtons whereas the range of drag for the turbulent flow environment is [2.109, 13.192] Newtons, as found from the team's data and **Fig. 4.1**. This is evidence that the drag is considerably higher under turbulent flow than laminar flow.

The purpose of this experiment is to maximize drag for PSP's Spaceport America rocket, which will be traveling at high altitudes and at higher speeds. In order to analyze the airbrake's performance under these conditions, the team used dimensional analysis and assumed dynamic and kinematic similarity. The geometric similarity was also assumed, however, it should be noted that the size of the test model is the same as the size of the prototype on PSP's Spaceport America rocket. Using the Buckingham-Pi theorem, the following Pi term was found to be a dimensionless drag force expression.

$$\pi_1 = \frac{F_D}{\rho V^2 A}$$

Under the assumptions of similarity, in addition to the simplifying assumptions made in **Section 1.1** and rearranging **Eqn. 5.1**, the velocity of the prototype can be found using the following relationship.

$$F_{D_P} = F_{D_M} \cdot \left(\frac{V_P}{V_M}\right)^2 \qquad \text{Eqn. 5.2}$$

In the derived expression above, the subscripts P and M represent the prototype and model, respectively. PSP Spaceport America's simulation has determined that the velocity of the rocket when the airbrake is intended to be deployed will 205.13 m/s. The velocity experienced by the model from testing was 44.66 m/s – this was the air velocity in the wind tunnel when the VFD was set to 60 Hz. Using the method of dimensional analysis, the maximum drag the prototype is expected to experience is 278.32N per airbrake at an angle of attack of 30°. This method was also repeated to find the minimum drag to be experienced by the airbrake when under laminar flow

conditions for an angle of attack of 5°. The range of drag for the prototype was thus found to be [3.155, 278.32] Newtons. Therefore, the ideal situation to maximize drag is an angle of attack of 30° with turbulent flow. Furthermore, the rocket is designed to have 3 airbrakes thus increasing the total maximum expected drag force to 834.96N. These are the design changes PSP should implement in order to maximize drag and reduce the rocket's apogee.

There are certain limitations involved with the experimental method. Firstly, when measuring drag at 0°, the team's results only measures drag above the air brake. However, some drag still acts underneath the airbrake in the exposed overhang surfaces on either side of the airbrake. Since this area is negligibly small and only exists at an angle of attack of 0°, it should offer negligible error to the data. This inaccuracy would mean that drag is slightly higher at 0° than what the results reflect.

In order to cancel out the drag that the frontal projection of the system induces, a second jug was printed to mimic the true model but without the airbrake. During calibration, the data from the jig is canceled out from the data read by the true model. Thus, the data accurately depicts the drag induced only by the top face of the airbrake, as it would in reality when mounted to the rocket. This calibration jig without the airbrake, due to a modeling error, was printed to be 0.1" taller than needed. This means that the drag measured for the calibration jig is slightly higher than the actual drag force it is intended to zero out. Therefore, the drag measured at an angle of attack of 0° is slightly lower than the actual value. Given that the first limitation causes the drag to be slightly larger, this second limitation negates some of that inaccuracy further reducing the error in the team's results, even if not completely.

Another limitation was that the experiment section of the wind tunnel was not large enough to test higher angles of attack. The team had the redesign the test setup by bending an all-thread rod to lower the position of the airbrake to allow it to even extend to an angle of attack of 30°. Because of these size constraints, the data to be collected was limited. This also meant there were multiple assemblies and disassembly of the model and test setup to collect the necessary data. As a result of this, minor imperfections and human error may have come forth when reassembling a test setup to match a previous experimental condition.

Furthermore, due to the nature of the complex design, additive manufacturing was the only efficient option. Limitations of the 3D printer nozzle prevented the team from designing an assembly with smaller gear teeth and more intricate details that would've allowed for data to be collected for angles of attack at step sizes lower than 5°.

A fourth limitation is that a singular airbrake was modeled as a streamline body but when in conjunction with 3 other airbrakes along the circumference of the rocket, it may better be represented as a bluff body and thus have a different frontal projection area. This would have thus resulted in different coefficient of drag values. However, the drag forces calculated would be the same. Since the drag force predictions are the most important data for the PSP team, this limitation can be noted but is ultimately irrelevant.

Finally, the last assumptions are to do with simplifying assumptions made. Air density changes with altitudes but since the difference is negligibly small relative to the drag forces being calculated, it can be treated as a constant value. The discrepancies in air density and other minor assumptions made by the team may even possibly be smaller than the uncertainty of the results.

In conclusion, many of the limitations offered minor and negligible imperfections to the data. Ultimately, the required data was found and is consistent with the team's predictions and scientific theories presented by academia. The PSP Spaceport America team will be able to use these findings to successfully design the airbrake system on their rocket to meet apogee goals.

REFERENCES

1. A.I.R.B.R.A.K.E.S - Kerbal Space Program Wiki. (2023). Retrieved 22 April 2023, from https://wiki.kerbalspaceprogram.com/wiki/A.I.R.B.R.A.K.E.S#:~:text=This%20is%20especially%20useful%20for,by%20selective%20deploying%20and%20undeploying
2. Tec-Science. (2021, April 26). *Flow separation (boundary layer separation) - tec-science*. tec. Retrieved April 21, 2023, from https://www.tec-science.com/mechanics/gases-and-liquids/flow-separation-boundary-layer-separation/

APPENDIX

APPENDIX A: CONTRIBUTION OF TEAM MEMBERS

The contributions to this report for each team member can be seen below:

Item\Name	Misenar, Joe	Tharun, Agathiya	Madhavan, Pranav	Subtotal
Project Idea	30%	50%	20%	100%
Proposal Preparation	45%	25%	30%	100%
Lab Test	34%	33%	33%	100%
Data Processing	20%	30%	50%	100%
Report Writing				
Introduction	10%	30%	60%	100%
Objective	60%	20%	20%	100%
Method	50%	20%	30%	100%
Results	15%	65%	20%	100%
Discussion	20%	30%	50%	100%
Edit & proofread	34%	33%	33%	100%
PPT preparation	33%	34%	33%	100%

APPENDIX B: CAD DRAWINGS

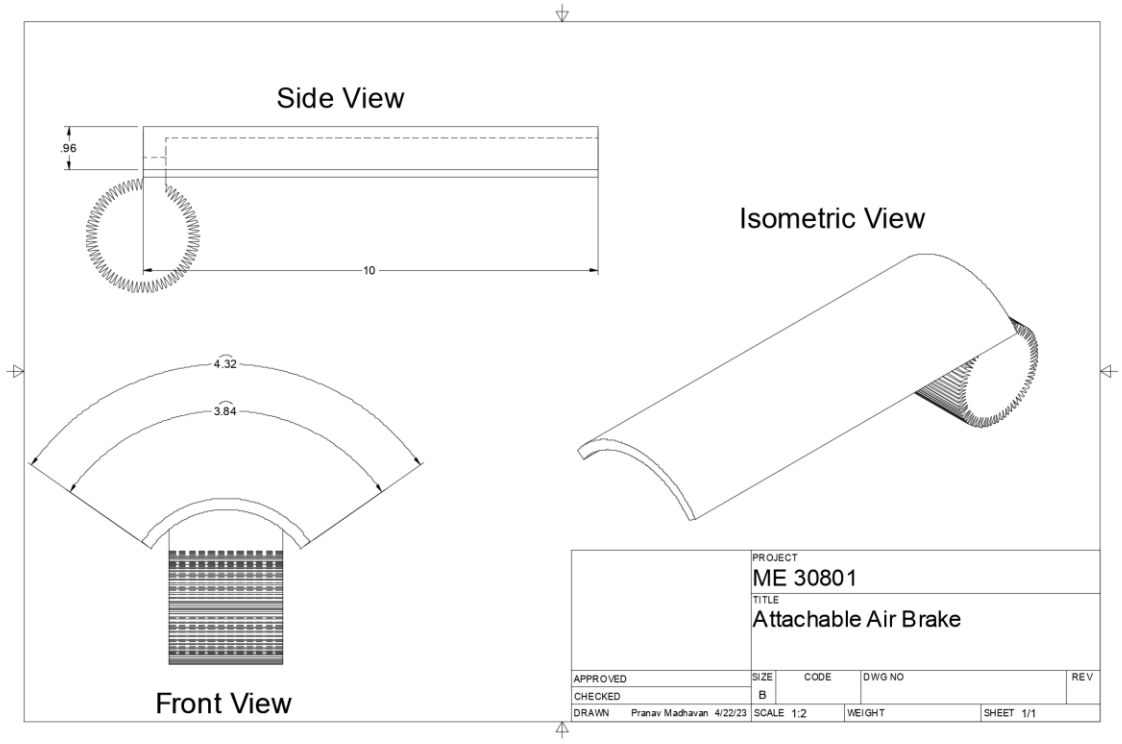

Fig. B.1 CAD Drawing of airbrake model.

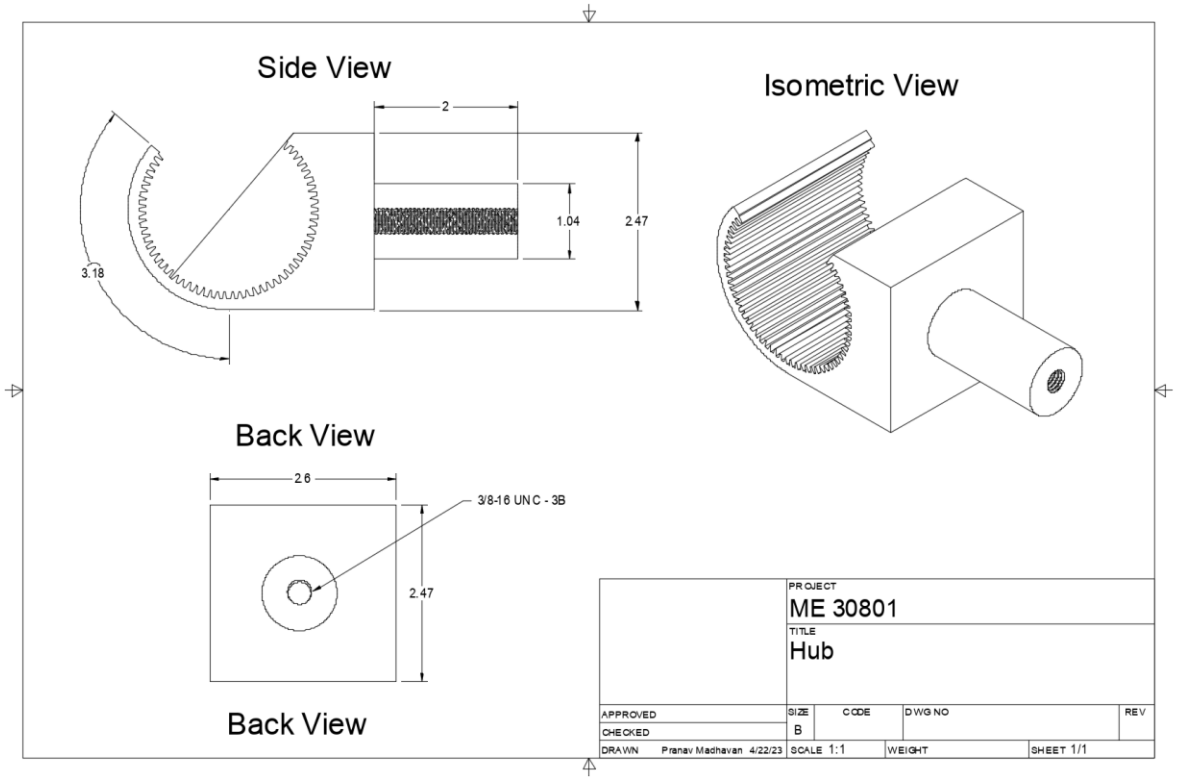

Fig. B.2 CAD Drawing of attachment hub.

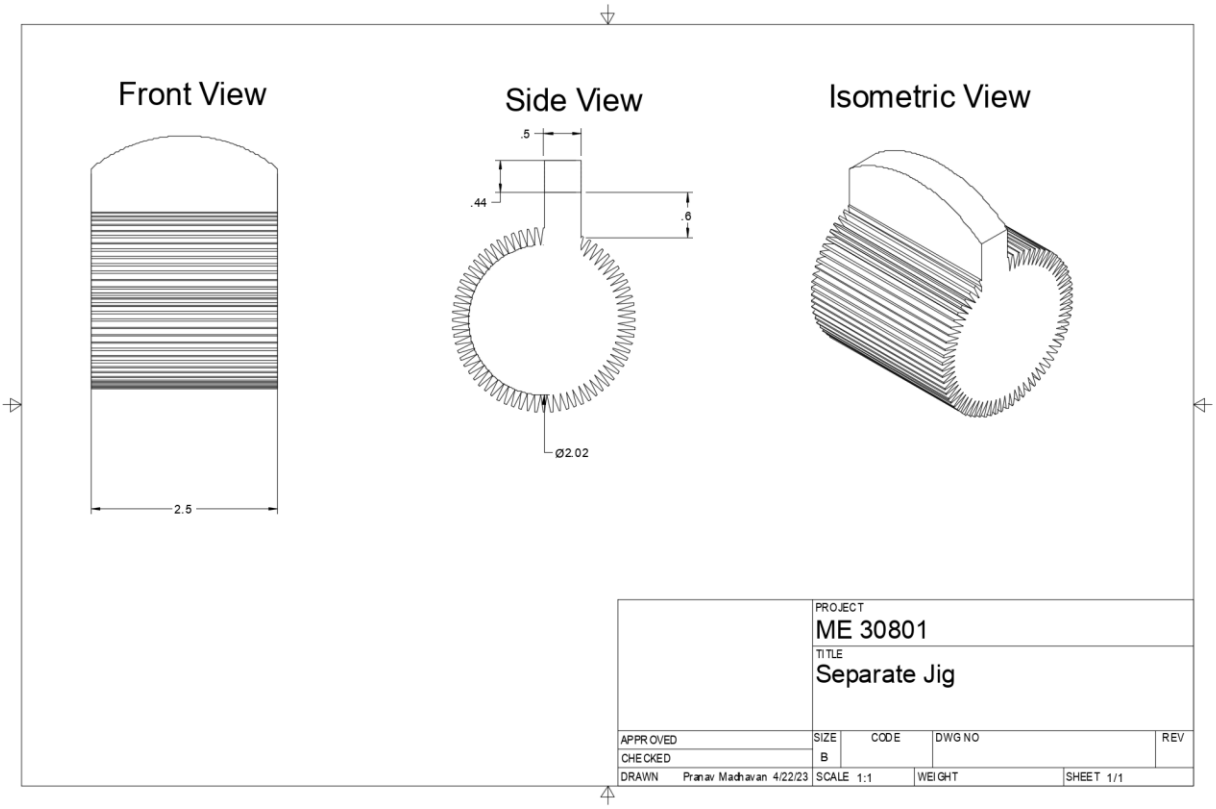

Fig. B.3 CAD Drawing of calibration jig.

APPENDIX C: CAD MODELS

The CAD Models corresponding to the drawings shown in **Appendix B** can be seen below.

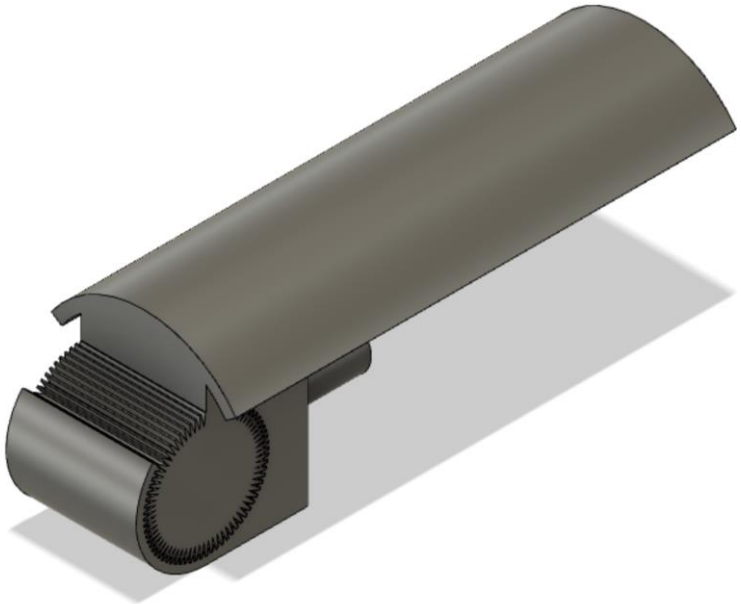

Fig. C.1 CAD model of airbrake.

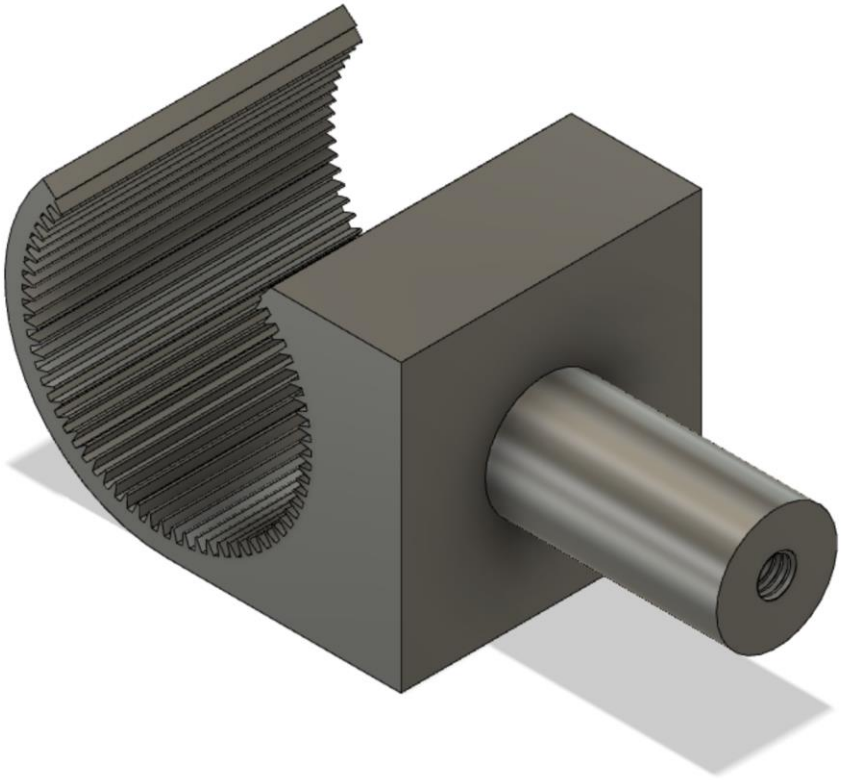

Fig. C.2 CAD model of attachment hub.

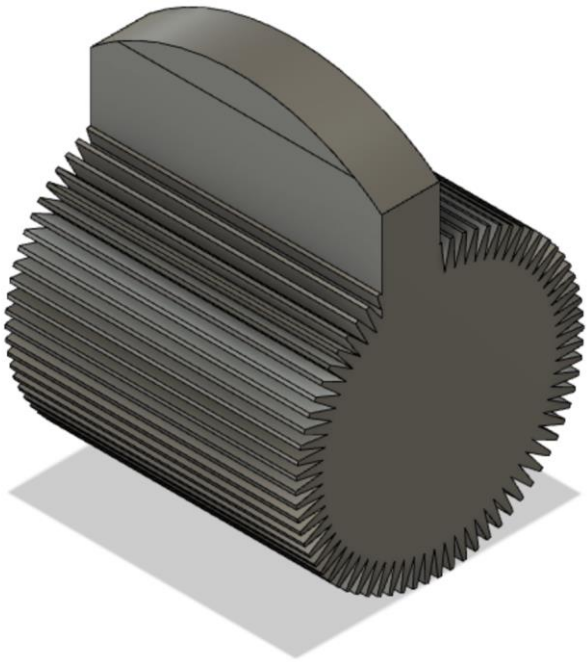

Fig. C.3 CAD model of calibration jig.